Surface Science 646 (2016) 126–131

Contents lists available at ScienceDirect

Surface Science

journal homepage: www.elsevier.com/locate/susc

Evolution of the electronic structure during the epitaxial growth of Au on Pt(100)

S. Bengió [a], L. Walczak [b], I. Vobornik [c], P. Segovia [b,d], E.G. Michel [b,d,*]

[a] Consejo Nacional de Investigaciones Científicas y Técnicas (Conicet) and Centro Atómico Bariloche, 8400 Bariloche, Argentina
[b] Departamento de Física de la Materia Condensada, Universidad Autónoma de Madrid, 28049 Madrid, Spain
[c] CNR-IOM, TASC Laboratory, AREA Science Park — Basovizza, SS14, km 163.5, IT-34149 Trieste, Italy
[d] Condensed Matter Physics Center (IFIMAC), Universidad Autónoma de Madrid, 28049 Madrid, Spain

ARTICLE INFO

Available online 31 August 2015

Keywords:
Au film surface
Electronic band structure
Pt(100)
Quantum well states
One dimensional surface states

ABSTRACT

We report an angle-resolved photoemission study of the electronic structure of Au layers grown epitaxially on Pt(100) in the coverage range 1–10 monolayers (ML). Our results include an analysis of the electronic band structure and the Fermi surface, combined with structural information from low-energy electron diffraction. The Au films grow epitaxially with a (1×1) pattern up to 4–5 ML. We monitor the electronic band structure near the surface $\bar{X}$-point vs. Au coverage. In the 1–3 ML range we observe interface electronic states related to the formation of a Au–Pt alloy in this coverage range. Starting at 2–3 ML coverage, we identify quantum well states from the incipient Au *sp* band, which converge into a bulk like Au *sp* band near 6 ML. After 5–6 ML, a (1×7) pattern is observed, due to the formation of a surface reconstruction in the epitaxial Au film with a topmost hexagonal layer, as in the reconstruction of bulk Au(100). We identify specific electronic states of quasi-one-dimensional character coming from the corrugated hexagonal layer. We obtain a complete picture and understanding of the electronic structure of Au/Pt(100), including *sp* Au band formation, hybridization and electronic confinement, and with implications in the understanding of the distinct electronic behavior of Au layers and particles in the nm size range.

1. Introduction

Low-dimensional systems have received ample attention during many years due to their exciting new physics and also to the many potential technological applications. In recent years, advances in experimental techniques have made possible a much deeper understanding of their properties. The electronic and structural properties of Au, Pt and their alloys have been a subject of continuous interest, due to their interesting features, including complex reconstructions [1-8], catalytic activity [9-11] and a specific electronic behavior [12,13]. The clean surfaces of Pt(100), Ir(100) and Au(100) prepared under adequate conditions in ultra-high vacuum are characterized by a complex surface reconstruction with a topmost layer of hexagonal symmetry [1-3]. The mismatch between the hexagonal layer and the substrate generates a strain that is released by lateral contraction and buckling of the hexagonal layer. In the case of Au(100), the topmost hexagonal layer is highly modulated in the $[\bar{1}10]$ direction, with a five-fold periodicity. In the [110] direction, there is a smooth modulation that leads to fringes with a chain-like structure and a much longer periodicity, in the range of $\times 26$ to $\times 28$ [4,5].

The Pt(100) surface exhibits two different phases of the reconstruction (see Ref. [8] and references therein). The first one is obtained upon annealing up to 1100 K and corresponds to an unrotated hexagonal top surface layer, Pt(100)-hex. Annealing above 1100 K stabilizes a new phase where the hexagonal layer is rotated 0.7° with respect to the square lattice, Pt(100)-hex-R0.7°. The properties of thin films of Au grown epitaxially on reconstructed Pt(100) have attracted attention due to several reasons. First, the growth of Au removes the Pt(100) reconstruction, while maintaining an overall good crystalline quality for many layers [14]. In fact, Au films thicker than 5–6 monolayers (MLs) exhibit a surface reconstruction similar to bulk Au(100). Second, this interface presents also an enhanced reactivity for Au thicknesses in the 1–2 ML range [15-17], a fact that might be related with the unique behavior of Au films and particles of nm size [9]. Earlier work on this interface characterized the growth mode, found the formation of a reconstructed Au top layer, and identified specific electronic states at the interface [14–16,18–21]. Using STM (Scanning Tunneling Microscopy), the growth process was described in great detail [22]. The Au film grows epitaxially with a (1×1) termination up to 4–5 ML. The first 2 ML of Au grow simultaneously, forming elongated Au islands with a Pt content in the range of 20%. The islands later coalesce into a two-dimensional film. Further growth is layer by layer, and soon (5–6 ML) the Au surface presents a (1×7) reconstruction, corresponding to a hexagonal surface termination. At this point, the reconstruction may

* Corresponding author at: Departamento de Física de la Materia Condensada, Universidad Autónoma de Madrid, 28049 Madrid, Spain.

http://dx.doi.org/10.1016/j.susc.2015.08.026
0039-6028/

have a predominant domain, probably due to strain in the epitaxial layer and to the existence of a preferred direction at the surface to diminish the strain, related with the natural surface steps.

In this work we set out to revisit the electronic structure of the Au/Pt/(100) system using Angle-Resolved Photoemission (ARPES) and Fermi surface mapping with the goal of understanding the electronic behavior of the thin Au layers and to determine how their structural properties affect the electronic states and their periodicity.

2. Experiment

Two different ultrahigh vacuum chambers (base pressure below 1×10^{-10} mbar) were used to perform ARPES and low-energy electron diffraction (LEED) experiments. The first apparatus receives He I and He II radiation from a plasma source (Gammadata) and uses a Phoibos 150 electron analyzer. The second chamber is located at the low-energy branch of the APE-IOM beamline [23], receiving synchrotron light from the Elettra storage ring (Trieste, Italy). It is equipped with a Scienta SES-2002 electron energy analyzer. The energy resolution was set to 20 meV and the angle resolution was better than 0.1°. A complete characterization of the electronic band structure was obtained using linearly polarized light (vertical and horizontal planes) with photon energies in the range from 34 to 84 eV, in a window of approximately 3.0 eV below the Fermi energy. Fermi surface mapping was performed at constant photon energy.

The Pt(100) sample was cleaned by cycles of 1 keV eV Ar ions sputtering, heating in oxygen (~700 °C and 1×10^{-8} mbar) and annealing in vacuum (850 °C) until the surface was free of contaminants and a sharp LEED pattern was observed, showing the characteristic spots of the Pt(100)-hex-R0.7° reconstruction. Au was deposited from a Knudsen cell and its coverage (Θ) was calibrated from the Au 4*f*/Pt 4*f* intensity ratio measured with $h\nu = 120$ eV and from the change in surface work function [18]. The estimated error of the coverage is ±15%. Electronic band structure and constant energy surface contours were simulated using the ELAN code [24]. In this code the Slater–Koster (SK) tight binding approach [25] is used as an interpolation method to generate the band dispersion $E(k)$ at a large number of k-points for a given structure.

3. Results

In agreement with previous reports for this interface [14,22], we find that the deposition of submonolayer amounts of Au removes the Pt(100) reconstruction. The LEED pattern is (1×1) up to 4–5 ML. At $\Theta_{Au} = 4$ ML the LEED pattern shows streaks, that evolve into a (1×7) pattern seen for $\Theta_{Au} > 5$ ML. This reconstruction is due to the formation of a topmost hexagonal layer on top of the square epitaxial Au(100) layers, and is analogous to the reconstruction observed for bulk Au(100) surfaces [14,22].

Fig. 1 shows the energy distribution curves (EDCs) corresponding to the valence band measured for normal emission as a function of Au coverage, from submonolayer up to several monolayers of Au. The clean Pt valence band (Fig. 1a) is dominated at $h\nu = 34$ eV by a high density of states coming from the *d* band, which appear near the Fermi energy. Upon Au deposition, the Pt *d* states are attenuated and cannot be distinguished above ~2–3 ML, Fig. 1e,f. For higher Au coverage (Fig. 1g,h), the *d* states of Au are seen in the −2 to −5 binding energy (BE) range. An additional band of Au is seen near −6 eV BE. The region closer to the Fermi energy (0 to −2 eV BE) is fairly flat, as the Au *sp* bulk band is not seen for the detection conditions of Fig. 1. Between the extreme spectra of clean Pt (Fig. 1a) and a layer of several MLs of Au (Fig. 1g,h) an intermediate range with specific behavior is observed (Fig. 1b–e), corresponding to Au coverages up to 2.5 MLs. In this range, two additional electronic states appear at −2 and −3 eV BE. The state at −2 eV BE is seen up to ~2.5 ML, while the second state at −3 eV is mixed with Au *d* states in the same coverage range.

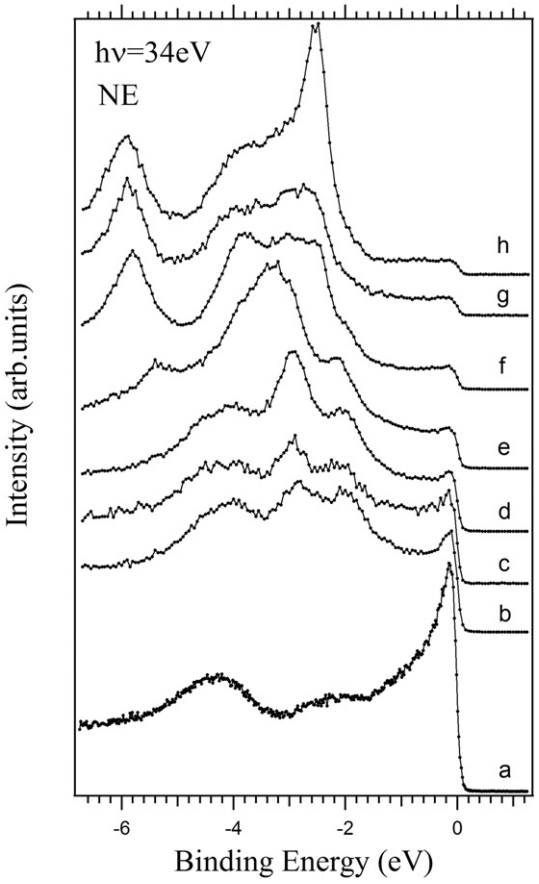

Fig. 1. Normal emission EDC's taken with $h\nu = 34$ eV for increasing Au coverages: a) clean Pt(100), b) 0.8 ML, c) 1.0 ML, d) 1.8 ML, e) 2.5 ML, f) 4.0 ML, g) 5.0 ML, h) 6.0 ML. For EDCs b–e, two interface states are observed at −2.0 and −2.8 eV BE.

Fig. 2 shows two sets of BE vs. parallel momentum ARPES dispersion maps, taken with $h\nu = 34$ eV and $h\nu = 84$ eV along $\overline{\Gamma X}$ direction. For each photon energy, the valence band region near $\overline{X}$ point is shown for increasing Au coverages. This region is favorable to observe the electronic states of the Au layer, as Pt(100) presents a *sp* band gap near it. Note that both sets correspond to approximately the same range along $\overline{\Gamma X}$ direction near the $\overline{X}$ point, but as they are taken with different photon energies, the corresponding values of the perpendicular momentum are very different. Bulk bands (dispersing with perpendicular momentum) are expected to appear at different reciprocal space locations in each set, while two dimensional bands should not disperse with photon energy. Both Pt and Au *sp* bands are identified by comparison of Fermi surface contours with calculations (see below).

Fig. 2a,b, corresponding to clean Pt(100) and $\Theta_{Au} = 1$ ML respectively, show the *sp* band of Pt (band nr. 6) crossing the Fermi energy near 0.8 $Å^{-1}$ (for $h\nu = 34$ eV) and 1.4 $Å^{-1}$ (for $h\nu = 84$ eV). Fig. 2f, corresponding to a thicker Au layer (6 ML) shows the *sp* band of Au crossing the Fermi energy near the $\overline{X}$ point. Note the change of bulk bands with photon energy (perpendicular momentum), consistent with their expected reciprocal space dispersion. We consider now the intermediate coverage range of Au (1.8 to 4.0 ML Au in Fig. 2, panels c, d, e). Here, together with the *sp* band of Pt, additional bands related to the thin Au film are observed. The most intense one is a band backfolded at the $\overline{X}$ point (panels c and d), and labeled A. A second weaker band (labeled B) is seen near the Fermi energy. Both bands (A and B) converge in panel e, to become the Au sp band seen in panel f. Bands A and B do not disperse with photon energy, denoting a two dimensional character, in agreement with the observed backfolding at the $\overline{X}$ point. On the other hand, the topmost BE of band A (corresponding

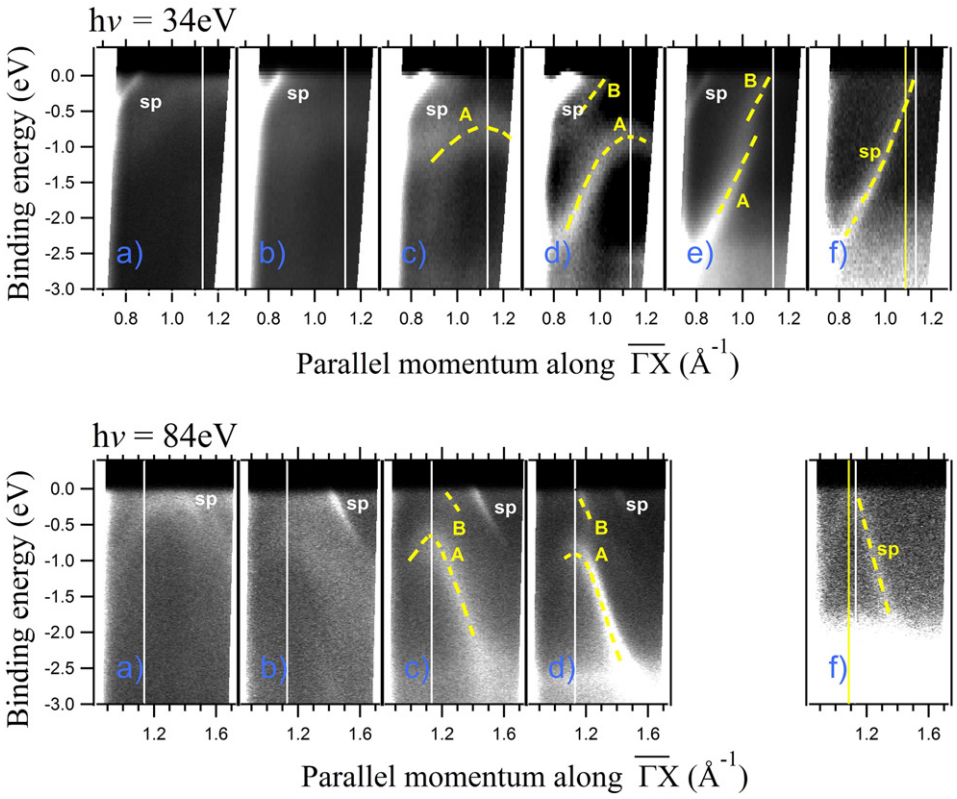

Fig. 2. ARPES dispersion maps (BE vs. parallel momentum along $\overline{\Gamma X}$ direction) in the region near $\overline{X}$ for $h\nu = 34$ eV (top panels) and for $h\nu = 84$ eV (bottom panels) as a function of Au coverage: a) clean Pt(100) surface, b) 1.0 ML, c) 1.8 ML, d) 2.5 ML, e) 4.0 ML, f) 6.0 ML. Panels labeled with the same letter correspond to the same Au coverage. Light color means higher intensity. The vertical white and yellow lines indicate the $\overline{X}$ symmetry point of Pt(100) (all panels) and Au(100) (f panel), respectively. Labels indicate the orbital origin of the different bands identified in white (yellow) for Pt (Au). Dashed lines are a guide to the view. Note the convergence of electronic states A and B of Au seen at intermediate coverages (panels c, d and e) into the Au *sp* band in panel f.

to the backfolding at the $\overline{X}$ point) depends on Θ and is slightly deeper for panel d than for panel c. There are several possible explanations for these electronic states, like surface or interface states associated to the two-dimensional Au layer, electronic states affected by the lateral confinement in the elongated Au islands observed for low coverages [22], or finally quantum-well-states (QWS) in the thin Au layer. An analysis of the experimental behavior of bands A and B, including their clear two dimensional character, dependence of the BE with coverage, similar

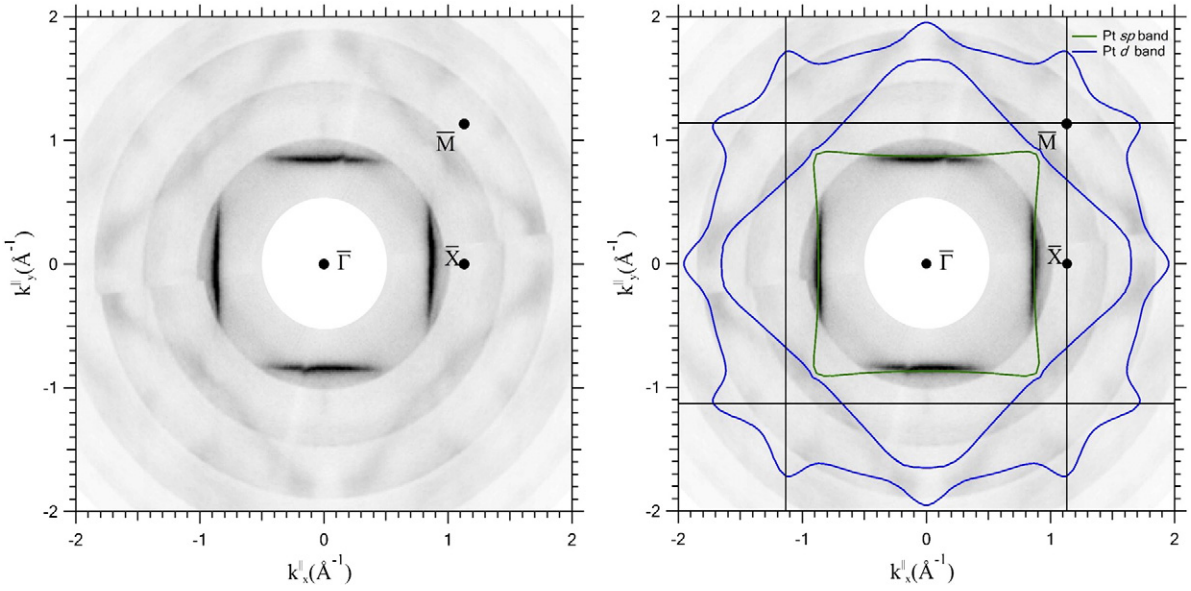

Fig. 3. Left panel: Fermi surface map of the Au/Pt(100) interface for $\Theta_{Au} \approx 0.8$ ML measured at $h\nu = 34$ eV. Experimental data are measured for 180° and symmetrized. Symmetry points correspond to the Pt(100) surface Brillouin zone. Right panel: theoretical Pt *sp* (band nr. 6) and Pt *d* (band nr. 5) contours are superimposed in green (*sp* band) and blue (*d* band). Concentric circles are an artifact due to the data acquisition method.

dispersion, and convergence of both bands into the *sp* band for larger coverages, supports that bands A and B are due to formation of QWS in the thin Au layer. These properties also discard any other possible explanations. QWS are seen clearly only near $\overline{X}$ point due to the partial *sp* band gap of Pt(100) in this reciprocal space region.

We analyze in the following the evolution of the Fermi surface of the interface as a function of coverage. The Fermi surface of the reconstructed Pt(100) surface presents a complex distribution of intensity, due to the band backfolding induced by the surface reconstruction and will not be analyzed here [26]. Fig. 3 shows the Fermi surface map of Pt(100) covered with 0.8 ML of Au. At this low coverage, the main effect of the Au layer is to remove the reconstruction of the Pt(100) surface. Additional electronic states induced by Au are not distinguished yet. In Fig. 3 (right) the theoretical *sp* and *d* bands are plotted as green and blue lines, respectively. The inner square corresponds to the Pt *sp* band, which presents higher intensity near the $\overline{X}$ points. The two outer contours correspond to Pt *d* bands and explain reasonably well the experimental intensities observed, taking into account that there might be still a residual folding due to reconstructed areas of the surface.

Fig. 4 shows the Fermi surface map of Pt(100) covered with 4.0 ML of Au. At this coverage the surface exhibits a streaked LEED pattern with incipient (1×7) spots. The electronic states coming from Pt(100) are still seen, partially attenuated by the Au layer. Besides these electronic states, new features due to the Au layer are observed. The yellow contour in Fig. 4 (right) highlights the Au *sp* band, which presents a shape similar to the Pt *sp* band, but with a slightly larger size. In addition to this, note the appearance in the Fermi surface map of weak straight lines, highlighted by the red dashed lines in Fig. 4 (right). These electronic states are seen more clearly near the $\overline{M}$ points. We recall at this point the findings made in a previous study on the electronic properties of reconstructed Au(100) [27]. The complex Fermi surface map of reconstructed Au(100) showed a contribution from the hexagonal topmost atomic layer of the reconstruction. The electronic states related to this layer present quasi-one-dimensional character, in agreement with the structure of the reconstructed layer, which is corrugated along one direction. Here, we observe the appearance of electronic features in the Fermi surface map with very similar properties in what concerns dispersion, periodicity and reciprocal space location. The nature and properties of these electronic states are seen even more clearly in Fig. 5, which shows a quadrant of the Fermi surface map of Au/Pt(100) for a coverage of 6 ML. Its LEED pattern corresponds to a (1×7) reconstruction almost single-domain, with weak streaks. The weak quasi-one-dimensional states seen in Fig. 4 are dominant for the coverage of Fig. 5. In agreement with the strong predominance of one of the two possible domains in the LEED pattern, the Fermi surface map shows also predominantly the quasi-one-dimensional electronic states related to one of the reconstruction domains. The Fermi surface map shows replicas of the electronic states with a lateral periodicity corresponding to $\Delta = 0.15\ \text{Å}^{-1}$.

As the bulk *sp* Au band is seen with high intensity near the $\overline{X}$ point, the quasi-one-dimensional electronic states are better seen near the $\overline{M}$ point, where there is less superposition of the bulk *sp* band coming from the Au(100) layers underneath. Fig. 6a shows an ARPES intensity map along $\overline{\Gamma M}$ direction taken near the $\overline{M}$ point, for $\Theta_{Au} = 10$ ML. The quasi-one-dimensional states exhibit a clear dispersion and several replicas are seen. Fig. 6b and c shows a schematic view of a one-dimensional free-electron-like surface state in an energy vs parallel momentum representation. Folding is expected along the $\overline{\Gamma X}$ direction (dispersing direction) with the periodicity of the reconstruction. As the ARPES intensity map in Fig. 6 is taken along $\overline{\Gamma X}$ direction the distances between the replicas are larger than along $\overline{\Gamma X}$ direction (Fig. 5, right panel).

4. Discussion

We find that the electronic structure of a thin Au layer grown epitaxially on reconstructed Pt(100) undergoes significant changes as function of coverage. The electronic states identified at each stage of the growth help to understand the specific properties of the Au layer. Previous work using core-level photoemission spectroscopy [22] identified different atomic contributions in the Au 4*f* core level, that were attributed to Au atoms at the interface with the Pt(100) surface, forming an alloy, Au surface atoms at the (1×1) terminated layer (observed for $\Theta \lesssim 4$ ML), and Au atoms at the (1×7) reconstructed surface.

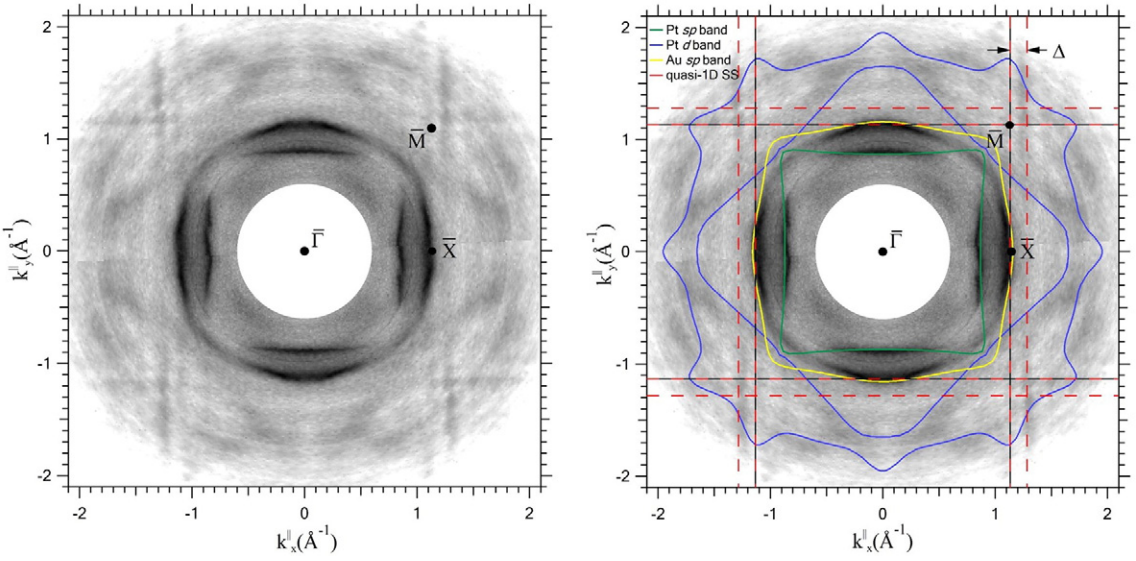

Fig. 4. Left panel: Fermi surface map of the Au/Pt (100) interface for $\Theta_{Au} \approx 4.0$ ML measured at $h\nu = 34$ eV. Experimental data are measured for 180° and symmetrized. Symmetry points correspond to the Au/Pt (100) surface Brillouin zone. Right panel: continuous black lines mark zone edges, the theoretical Pt *sp* (band nr. 6) and Pt *d* (band nr. 5) contours are superimposed as green (*sp* band) and blue (*d* band) lines and the theoretical Au *sp* (band nr. 6) is superimposed as a yellow line. Red dashed lines highlight weak straight lines (vertical and horizontal), seen with more intensity near the $\overline{M}$ points and related to quasi one-dimensional electronic states. Concentric circles are an artifact due to the data acquisition method.

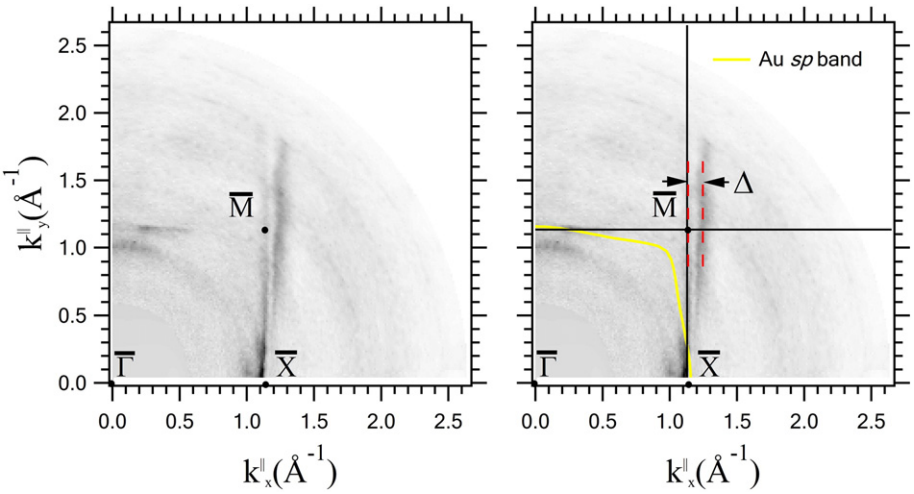

Fig. 5. Left panel: Fermi surface map of the Au/Pt(100) interface for Θ ≈ 6.0 ML measured at $h\nu = 34$ eV. Right Panel: zone edges and the theoretical Au sp band are superimposed in the Fermi surface. Symmetry points correspond to the Pt(100) surface Brillouin zone. Dashed red lines follow the straight lines of the quasi-one-dimensional states.

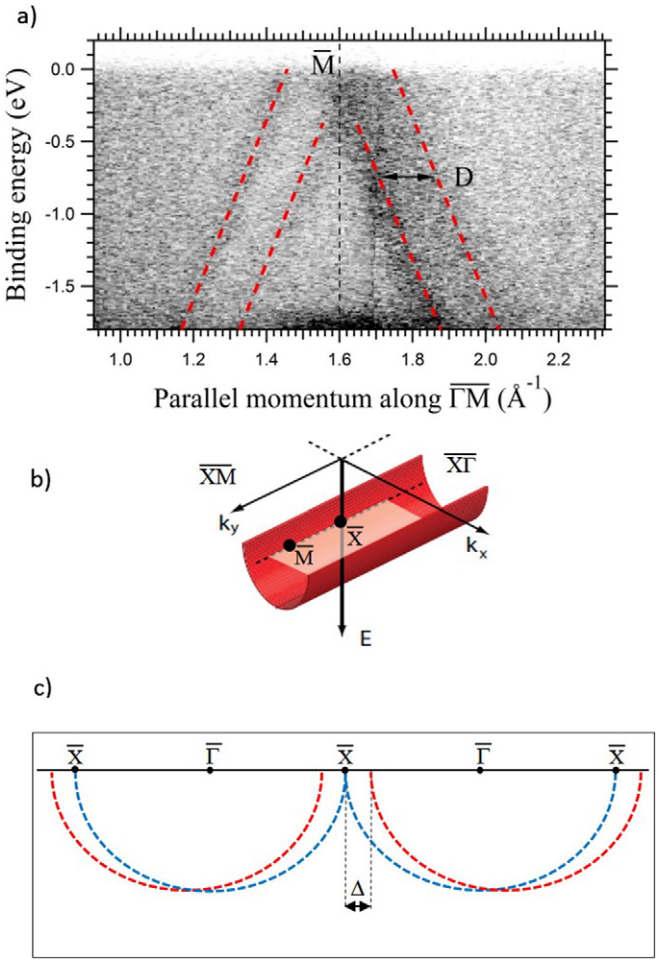

Fig. 6. Panel a): ARPES dispersion map (BE vs. parallel momentum along $\overline{\Gamma M}$ direction) of Au/Pt (100) (Θ = 10 ML) in the region near $\overline{M}$ for $h\nu = 84$ eV in gray scale (darker color means higher intensity). Red lines are a guide to the view. *D* measures the distance between split bands. Panels b) and c): schematic view of the dispersion of a one-dimensional electronic state (panel b) and its energy momentum representation along $\overline{\Gamma X}$ (panel c), showing original states (blue dashed lines) and superperiodicity induced replicas (red dashed lines). Δ (splitting along $\overline{\Gamma X}$ direction) is equal to $D \cos 45^{\circ}$.

Fig. 1 shows that the first two Au layers present different electronic states. As these states are not observed for thicker Au layers, they can be identified with electronic states specific of the first two Au layers. In this coverage range, the thin Au layer can be described as an alloy containing up to 20% of Pt atoms [22], and it should develop characteristic electronic states. Similar electronic states were seen in earlier work on this interface using angle-integrated valence band photoemission [18], and were related with the enhanced reactivity of the Au/Pt interface [15,16]. As the first and second Au MLs grow simultaneously [22], the specific features of the interface are observed for Au coverages smaller than 2 ML, in agreement with the observation in Fig. 1 of additional electronic states in this coverage range. This is also consistent with the enhanced intensity of the Pt *sp* band in panels b, c and d of Fig. 2 (up to 2.5 ML), that can be related to the formation of a Au–Pt alloy, as a result of hibridization involving also the Pt *sp* band. For even thicker layers up to 6 ML, we observe the formation of QWS in the thin Au layer. The formation of QWS is a frequent phenomenon during epitaxial growth of thin metallic films [28]. In principle, QWS are observed when electronic states of the growing film are confined between the vacuum barrier and a substrate band gap, although this condition is weakened in specific cases [29]. In the case of the Pt(100) surface, an area of *sp* band gap exists near the $\overline{X}$ point, which may explain why Au QWS are seen with sufficient intensity near this area. It is interesting to note that the evolution of the QWS seen in Fig. 2 shows a fairly fast convergence into the bulk band for a coverage of only 6 ML. Taking into account that the quality of the growth of the Au layer is good [22], this observation suggests that the electron confinement in the Au layer is only partial, as expected from the remarks made above.

An analysis of the Fermi surface contours of the Au/Pt(100) interface provides a deeper insight in the electronic properties of the Au layer. The Fermi surface of Fig. 3, which has no relevant contribution from Au electronic states due to the low coverage, shows features coming from the partially filled *sp* and *d* bands of Pt. Fig. 4 shows a mixture of electronic states from the Pt substrate and the thin Au layer. It is interesting to compare both *sp* bands from Pt and Au, exhibiting distinct sizes. The most remarkable feature is the appearance of electronic states showing quasi-one-dimensional behavior, which becomes dominant for a larger Au coverage and a fully reconstructed surface, as shown in Fig. 5. An interpretation of these states is facilitated by the observation of similar electronic states in the reconstructed surface of bulk Au(100) [27]. The topmost layer of the thin Au film is of hexagonal symmetry, and thus the surface of the film presents a reconstruction that resembles the one observed in bulk Au(100). We note here a

difference with respect to the bulk Au(100) crystal, where the surface reconstruction is fivefold along $[\bar{1}10]$ direction, and presents a longer periodicity (in the range of 26–28) in the [110] direction. The fivefold periodicity is due to the very good lattice match of 5 square unit cells with 6 hexagonal unit cells for Au, see e.g. Fig. 1 from Ref. [27]. As the epitaxial Au layers grow with the lateral lattice constant of Pt(100) [14], which is 4% smaller than the lattice constant of Au, the lattice match is now obtained for 7 square unit cells of strained Au (with the Pt lattice constant) with 8 hexagonal unit cells of Au, in good agreement with the observed sevenfold periodicity. It is clear that due to the different strain distributions, the longer periodicity could differ from the values observed in Au. Neither STM [22] nor LEED could determine the longer periodicity for the thicknesses studied in this work.

As in the case of Au(100), the top layer behaves as a system electronically decoupled from the substrate [27], due to the different crystalline symmetry. It presents quasi-one-dimensional electronic electronic states confined within the reconstruction fringes, so that they are delocalized and quasifree electrons along k_x in Fig. 5 (see also Fig. 6), while they are confined, and thus present constant BE vs parallel momentum along k_y. This interpretation is supported by an analysis of the electronic states, which present all the specific features expected, including dispersion/localization along the right reciprocal space directions, and backfolding with the reconstruction superperiodicity, as seen in Figs. 4, 5 and 6. The distance between the replicas along $\overline{\Gamma X}$ is 0.11 $Å^{-1}$. Taking $\Delta = 2\pi/na$, being $a = 2.77$ Å the square lattice constant of Pt(100), the superperiodicity observed corresponds to $n = 21$. This is similar to the values found in bulk Au(100). A comparison with this case reveals several interesting features. First, at variance with bulk Au(100), the bulk bands of the thin Au film are not completely formed yet and in any case there is a much smaller number of atomic layers contributing to the bulk part of the electronic structure. Furthermore, the Au surface state observed near the $\overline{X}$ point of bulk Au(100) is not yet seen. The presence of all these electronic states prevented in the case of bulk Au(100) the observation of the quasi-one-dimensional states in the region closer to the Fermi energy. In turn, the dispersion of the quasi-one-dimensional states seen in the Au/Pt(100) case can be monitored in the near Fermi energy region, especially near the $\overline{M}$ point, as shown in Fig. 6. Using this information, we consider now the possible role of the quasi-one-dimensional state in triggering and stabilizing the reconstruction. Such a hypothesis has been observed in other systems [30] and was put forward in the case of Au(100) on the basis of several compelling experimental observations, in particular the finding of a "magic" width of the reconstruction fringes equal to 14.4 Å, which corresponds to 5 atomic rows. As this width should correspond to the maximum energy win by formation of the reconstruction, it was speculated that it could minimize the electronic energy of the hexagonal layer. In fact, it is clear in Fig. 6 that the crossing point of the quasi-one-dimensional states is at the $\overline{XM}$ symmetry line, which is the requirement for a gap opening at the Fermi energy. Unfortunately, the weak intensity of the electronic states does not permit to conclude whether a gap opens or not at the $\overline{XM}$ symmetry line, but the hypothesis is very tempting.

5. Conclusions

We have studied the electronic structure of the Au/Pt(100) system for Au coverages up to 10 ML with ARPES and LEED. We have identified electronic states characteristic of the different stages of the growth. For coverages <2.5 ML we observe interface states related to the Au–Pt alloy formed. For thicker Au films up to 6 ML we identify the appearance of QWS in the thin Au film, which evolve with coverage and converge into the *sp* band. As soon as the thin Au layer exhibits a surface reconstruction, we observe quasi-one-dimensional electronic states, associated with the reconstruction fringes. As in the case of bulk Au(100), the existence of these electronic states is made possible by the lateral corrugation of the reconstructed layer and its electronic decoupling from the bulklike Au film of square symmetry underneath. The quasi-one-dimensional states replicate with the reconstruction periodicity. We analyze their possible role in triggering and stabilizing the reconstruction. We conclude that the rich electronic structure of Au/Pt(100) films is a suitable laboratory to test dimensionality effects and the interplay between surface and volume electronic structure.

Acknowledgment

This work was funded by MINECO under grant FIS2011-23230. The research leading to these results has received funding from the European Community's Seventh Framework Programme (FP7/2007-2013) CALIPSO under grant agreement nr. 312284. We thank A. Mascaraque for fruitful discussions and the critical reading of the manuscript.

References

[1] M.A. Van Hove, R.J. Koestner, P.C. Stair, J.P. Bibérian, L.L. Kesmodel, I. Bartŏs, G.A. Somorjai, Surf. Sci. 103 (1981) 189.
[2] M.A. Van Hove, R.J. Koestner, P.C. Stair, J.P. Bibérian, L.L. Kesmodel, I. Bartŏs, G.A. Somorjai, Surf. Sci. 103 (1981) 218.
[3] P. Heilmann, K. Heinz, K. Müller, Surf. Sci. 83 (1979) 487.
[4] B.M. Ocko, D. Gibbs, K.G. Huang, D.M. Zehner, S.G.J. Mochrie, Phys. Rev. B 44 (1991) 6429.
[5] D. Gibbs, Phys. Rev. B 42 (1990) 7330.
[6] Y.-F. Liew, G.-C. Wang, Surf. Sci. 227 (1990) 190.
[7] K. Yamazaki, K. Takayanagi, Y. Tanishiro, K. Yagi, Surf. Sci. 199 (1988) 595.
[8] G. Ritz, M. Schmid, P. Varga, A. Borg, M. Ronning, Phys. Rev. B 56 (1997) 10518.
[9] M. Chen, Y. Cai, Z. Yan, D.W. Goodman, J. Am. Chem. Soc. 128 (2006) 6341.
[10] G.C. Bond, Platin. Met. Rev. 51 (2007) 63.
[11] S.A. Tenney, W. He, J.S. Ratliff, D.R. Mullins, D.A. Chen, Top. Catal. 54 (2011) 42.
[12] A. Bendounan, K. Aït-Mansour, J. Braun, J. Minár, S. Bornemann, R. Fasel, O. Gröning, F. Sirotti, H. Ebert, Phys. Rev. B 83 (2011) 195427.
[13] B. Gu, I. Sugai, T. Ziman, G.Y. Guo, N. Nagaosa, T. Seki, K. Takanashi, S. Maekawa, Phys. Rev. Lett. 105 (2010) 216401.
[14] J.W.A. Sachtler, M.A. Van Hove, J.P. Biberian, G.A. Somorjai, Surf. Sci. 110 (1981) 19.
[15] J.W.A. Sachtler, M.A. Van Hove, J.P. Biberian, G.A. Somorjai, Phys. Rev. Lett. 45 (1980) 1601.
[16] J.W.A. Sachtler, J.P. Biberian, G.A. Somorjai, Surf. Sci. 110 (1981) 43.
[17] Y. Iijima, T. Kondo, Y. Takahashi, Y. Bando, N. Todoroki, T. Wadayama, J. Electrochem. Soc. 160 (2013) F898.
[18] M. Salmeron, S. Ferrer, M. Jazzar, G.A. Somorjai, Phys. Rev. B 28 (1983) 1158.
[19] M. Salmeron, S. Ferrer, M. Jazzar, G.A. Somorjai, Phys. Rev. B 28 (1983) 6758.
[20] S.C. Wu, C.K.C. Lok, S.H. Lu, J. Quinn, D. Tian, Y.S. Li, F. Jona, Phys. Rev. B 38 (1988) 7448.
[21] D.-S. Wang, A.J. Freeman, H. Krakauer, Phys. Rev. B 29 (1988) 1665.
[22] C. Berg, H.J. Venvik, F. Strisland, A. Ramstad, A. Borg, Surf. Sci. 409 (1998) 1.
[23] G. Panaccione, et al., Rev. Sci. Instrum. 80 (2009) 043105.
[24] V. Joco, N. Mikuszeit, J. Martínez-Blanco, E. G. Michel, to be published.
[25] J.C. Slater, G.F. Koster, Phys. Rev. 94 (1954) 1498.
[26] S. Bengió, L. Walczak, I. Vobornik, P. Segovia, E.G. Michel, in preparation.
[27] S. Bengió, V. Navarro, M.A. González-Barrio, R. Cortés, I. Vobornik, E.G. Michel, A. Mascaraque, Phys. Rev. B 86 (2012) 045426.
[28] M. Milun, P. Pervan, D.P. Woodruff, Rep. Prog. Phys. 65 (2002) 99 and references therein.
[29] T.R.J. Bollmann, R. van Gastel, H.J.W. Zandvliet, B. Poelsema, New J. Phys. 13 (2011) 103025.
[30] T.F. Mocking, P. Bampoulis, N. Oncel, B. Poelsema, H.J.W. Zandvliet, Nat. Commun. 4 (2013) 2387.